Available online at www.sciencedirect.com
ScienceDirect
Geochimica et Cosmochimica Acta 70 (2006) 4436–4451
Geochimica
www.elsevier.com/locate/gca

Effect of pH and organic ligands on the kinetics of smectite dissolution at 25 °C

Sergey V. Golubev [a], Andreas Bauer [b], Oleg S. Pokrovsky [a,*]

[a] Aqueous Experimental Geochemistry and Biogeochemistry Group, UMR 5563 CNRS—Observatoire Midi-Pyrénées, Université Paul-Sabatier, 14 Avenue Edouard Belin, 31400 Toulouse, France

[b] Forschungszentrum Karlsruhe, Institut für Nukleare Entsorgung, INE, P.O. Box 3640, 76021 Karlsruhe, Germany

Received 11 October 2005; accepted in revised form 29 June 2006

Abstract

Forward dissolution rates of Na–Montmorillonite (Wyoming) SWy-2 smectite $(Ca_{0.06}Na_{0.56})[Al_{3.08}Fe(III)_{0.38}Mg_{0.54}][Si_{7.93}Al_{0.07}]O_{20}(OH)_4$ were measured at 25 °C in a mixed-flow reactor equipped with interior dialysis compartment (6–8 kDa membrane) as a function of pH (1–12), dissolved carbonate (0.5–10 mM), phosphate (10^{-5} to 0.03 M), and nine organic ligands (acetate, oxalate, citrate, EDTA, alginate, glucuronic acid, 3,4-dihydroxybenzoic acid, gluconate, and glucosamine) in the concentration range from 10^{-5} to 0.03 M. In organic-free solutions, the Si-based rates decrease with increasing pH at $1 \leqslant pH \leqslant 8$ with a slope close to −0.2. At $9 \leqslant pH \leqslant 12$, the Si-based rates increase with a slope of ~0.3. In contrast, non-stoichiometric Mg release weakly depends on pH at $1 \leqslant pH \leqslant 12$ and decreases with increasing pH. The empirical expression describing Si-release rates [R, mol/cm^2/s] obtained in the present study at 25 °C, $I = 0.01$ M is given by

$$R = 2.2 \cdot 10^{-17} \cdot a_{H^+}^{0.21} + 1.0 \cdot 10^{-20} + 6 \cdot 10^{-17} \cdot a_{OH^-}^{0.33}$$

At circum-neutral pH, the Si-release-based dissolution is promoted by the addition of the following ligands ranked by decreasing effectiveness: EDTA > 3,4-DHBA > citrate ⩾ oxalate. Phosphate, glucuronate, glucosamine, gluconate, alginate, and acetate act as inhibitors of dissolution and HCO_3^-, CO_3^{2-} exhibit no effect on dissolution rate. Non-stoichiometric, non-steady-state Mg release was very weakly affected by the presence of ligands. Analysis of reacted solid products using XRD, FT-IR, and XPS revealed no major change in structure, surface chemical composition or specific surface area as a function of pH, ligand concentration, and duration of experiments. Ligand-affected rates re-calculated to constant pH were interpreted using a phenomenological equation which postulates the Langmurian adsorption of a ligand on surface sites. Overall, results of this study demonstrate that very high concentrations (0.001–0.01 M) of organic ligands, whether they are originated from organic matter enzymatic degradation or bacterial metabolic activity are necessary to appreciably affect smectite dissolution. As a result, the effect of natural organics on the weathering rate of smectite is expected to be weak.

1. Introduction

It is known that the weathering of Ca- and Mg-bearing silicates controls CO_2 uptake from the atmosphere and thus the climate of the earth at the long-term scale (Berner, 1992; Dupré et al., 2003). While the chemical weathering of "basic" primary silicate minerals (olivine, pyroxenes, basaltic glass, and anorthite) was fairly well characterized during the last 10 years (Sverdrup, 1990; Wogelius and Walther, 1991; Brady and Carroll, 1994; Lasaga, 1995; Brady and Gíslason, 1997; Berg and Banwart, 2000), the reactivity of secondary silicate clays except, probably, kaolinite (i.e., Carroll and Walther, 1990; Nagy et al., 1991; Wieland and Stumm, 1992; Devidal et al., 1997; Huertas et al., 1998, 1999; Metz and Ganor, 2001; Cama et al., 1999, 2002; Ganor et al., 2003) is still poorly known. Among these

* Corresponding author. Fax: +5 61332650.
E-mail address: oleg@lmtg.obs-mip.fr (O.S. Pokrovsky).

0016-7037/$ - see front matter © 2006 Elsevier Inc. All rights reserved.
doi:10.1016/j.gca.2006.06.1557

secondary clays, Ca-and Mg-bearing soil minerals (smectite and illite) are the most important for the balance of carbon dioxide consumption during rock weathering as follows from the Högbom (1894) reaction.

This work is a part of concerted efforts aimed at the quantitative characterization of physico-chemical factors controlling the reactivity of major "basic" soil- and rock-forming minerals in aqueous solutions at ambient temperatures. In previous works, we assessed the kinetics and mechanisms of olivine Mg_2SiO_4, brucite $Mg(OH)_2$, and wollastonite $CaSiO_3$ dissolution as a function of pH and concentration of various organic and inorganic ligands, notably dissolved carbonate (Pokrovsky and Schott, 2000b; Pokrovsky and Schott, 2004; Golubev et al., 2004, 2005; Pokrovsky et al., 2004, 2005a). This paper addresses the reactivity of smectite via experimental measurements of its dissolution rate at far from equilibrium conditions in the mixed-flow reactor in the wide range of pH and ligand concentrations. We attempted to assess, for the first time, the separate effect of pH, inorganic, and organic ligand concentration on Si, Mg, and Al mobilization rates from the reference sample of purified Na–montmorillonite.

Over the past 10 years, an extensive amount of information has been collected on macroscopic (i.e., Furrer et al., 1993; Zysset and Schindler, 1996; Bauer and Berger, 1998; Cama et al., 2000; Huertas et al., 2001; Metz et al., 2005a,b; Amram and Ganor, 2005) and microscopic (Bosbach et al., 2000; Bickmore et al., 2001) observation of smectite reactivity as a function of pH, temperature, and chemical affinity. These studies developed a comprehensive understanding of the phenomenological mechanisms that control smectite dissolution in inorganic systems. It is important to note that many previous works were performed with non-purified SAz-1 bentonite which contains around 8% of amorphous silica (Metz et al., 2005a,b; Amram and Ganor, 2005). To avoid the uncertainties associated with multicomponent character of the solid and various experimental artifacts related to the separation of <0.1 μm smectite crystals from solution using conventional 0.22–0.45 μm filters in earlier works, in this study we used specially purified endmember smectite SWy-2 separated from solution via <0.01 μm dialysis membrane. It is anticipated that results of the present study will enable a better description of smectite chemical weathering under naturally relevant conditions and will allow estimation of its effect on atmospheric CO_2 mass balance.

2. Materials and methods

2.1. Starting clay

The starting clay mineral for this experimental study was purified homoionic montmorillonite obtained from the SWy-1 source clay material (Clay Minerals Society, Purdue University, http://www.clays.org/sourceclays/SourceClays.html). In a first step the clay was conditioned to remove soluble salts, sparingly soluble minerals, and trace cation impurities following the procedure proposed by Bauer and Velde (1999). The purified smectite was converted into sodium form following Moore and Reynolds (1997) and the <0.1 μm fraction of smectite was separated via centrifugation and freeze-dried for storage. XRD and chemical analysis for conditioned clay revealed montmorillonite SWy-2 with a chemical formula of:

$$(Ca_{0.06}Na_{0.56})[Al_{3.08}Fe^{(III)}_{0.38}Mg_{0.54}][Si_{7.93}Al_{0.07}]O_{20}(OH)_4$$

and the specific surface area (SSA) was equal to 48 m^2/g as measured by BET method (see Section 2.9).

2.2. Dissolution kinetics experiments

Steady-state dissolution rates were obtained at distinct solution compositions and pH using a mixed-flow reaction vessel equipped with a dialysis bag held at a constant temperature of 25.0 ± 0.5 °C by immersion in a thermostated water bath. The input fluid was stored in a polyethylene container protected against CO_2 uptake from the atmosphere. It was injected into the reaction vessel using a Gilson® peristaltic pump at typical flow rates 0.05–0.1 mL/min. The reactor consisted of a 250 mL Azlon® plastic beaker which was continuously stirred with a floating teflon supported magnetic stirrer. The reactive solution left the reactor through a 2.5 μm pore size polycarbonate filter. Between 0.3 and 0.8 g of smectite particles (<0.1 μm) in the form of suspension were enclosed in 10-mL dialysis bag (6–8 kDa, SpectraPor® 6). This dialysis bag was sealed and fixed between the stirrer and the reactor head. Similar design has been used by Kohler et al. (2005) during their long-term study of illite dissolution. Dialysis membrane does not allow the mineral particles or colloids to clog the filter for the outlet solution while it insures the identical composition of aqueous species inside the bag and in the outlet solution. Over long-term dissolution experiments, the equilibrium distribution of solutes between the content of the dialysis bag and the external solution was not a limiting factor for steady-state attainment: it takes typically 24–48 h to establish the dialysis equilibrium while the mechanical steady-state in the reactor system is achieved only after 200 h. For most experiments lasting 30–40 days each, one sampling per day was performed.

Steady-state dissolution rates ($R_{Si,Al}$, mol/cm^2/s) given in Table 1 were computed from measured solution composition using

$$R_i = -q \cdot 1/n \cdot \Delta[i(aq)]_{tot}/s \quad (1)$$

where q(L/s) designates the fluid flow rate, $\Delta[i(aq)]_{tot}$ (mol/L) stands for the difference between the input and output solution concentration of i-th element, n is the stoichiometric coefficient of i-th element in smectite formula equal to 8 and 3 for Si and Al, respectively and s(cm^2) refers to the total mineral surface area present in reactor. The surface area used to calculate the rates listed in Table 1 was that measured on the fresh (unreacted) smectite powder purified as described in Section 2.1. Uncertainties on the

Table 1
Summary of smectite SWy-2 dissolution experiments performed at 25 °C in mixed-flow reactors equipped with dialysis cell

Exp. Nos.	Duration, h	SSA final, m^2/g	Mass, g	Flow rate, ml/min	Composition	pH	[Ca], μM	[Mg], μM	[Al], μM	[Si], μM	log R_{Si}	log R_{Al}
S5-2	615	46	0.335	0.09	0.1 M HCl	1.1	N.D.	1.05	N.D.	11.2	−16.89	
S5-1	832		0.335	0.09	0.01 M HCl	2.1	0.7	2.3	0.55	9.3	−16.97	−17.77
S1	1222	53	0.347	0.09	0.01 M NaCl	3.0	0.82	1.39	0.18	5.62	−17.20	−18.27
S2	1222	50	0.335	0.09	0.01 M NaCl	5.5	0.76	0.95		1.47	−17.77	
S3	1222	49	0.331	0.09	0.01 M NaCl	10.5	N.D.	0.45	1.62	7.1	−17.08	−17.29
S4-1	832		0.349	0.09	10^{-5} M oxalate	4.1	0.88	0.96	<D.L.	1.5	−17.78	
S4-2	500		0.349	0.09	0.0001 M oxalate	6.48	N.D.	0.84	<D.L.	1.4	−17.81	
S4-3	325		0.349	0.09	0.001 M oxalate	7.05	N.D.	0.99	<D.L.	1.34	−17.83	
S4-4	283	50	0.349	0.09	0.01 M oxalate	7.1	0.6	1.37	<D.L.	2.36	−17.58	
S6-1	832		0.318	0.09	0.01 M NaCl + NaOH	11.7	0.3	0.12	2.64	8.25	−17.00	−17.06
S6-2	313		0.318	0.09	0.0001 M acetate	6.75	1.62	1.85	<D.L.	2.76	−17.47	
S6-3	237		0.318	0.09	0.001 M acetate	6.28	0.98	1.79	<D.L.	2.27	−17.56	
S6-4	283	54	0.318	0.09	0.01 M acetate	6.05	N.D.	1.28	<D.L.	1.29	−17.80	
S7-1	832		0.35	0.08	0.01 M NaCl	7.1	0.88	1.16	<D.L.	1.19	−17.93	
S7-2	500		0.35	0.08	0.0005 M $NaHCO_3$	7.6	N.D.	0.8	<D.L.	0.85	−18.08	
S7-3	325		0.35	0.08	0.003 M $NaHCO_3$	8.4	N.D.	0.64	<D.L.	1.09	−17.97	
S7-4	283	51	0.35	0.08	0.01 M $NaHCO_3$	8.58	0.84	0.59	<D.L.	0.81	−18.10	
S8-1	832		0.339	0.09	0.01 M NaCl	7.3	0.74	11.14	<D.L.	11.41	−17.79	
S8-2	500		0.339	0.09	0.0005 M Na_2CO_3	10.05	N.D.	00.26	N.D.	33.94	−17.34	
S8-3	325		0.339	0.09	0.001 M Na_2CO_3	10.5	N.D.	0.31	N.D.	44.21	−17.32	
S8-4	283	42.5	0.339	0.09	0.0033 M Na_2CO_3	10.8	N.D.	0.17	N.D.	55.53	−17.20	
S9-1	570		0.735	0.07	10^{-5} M citrate	6.3	0.3	2.00	N.D.	3.2	−17.88	
S9-2	170		0.735	0.068	10^{-4} M citrate	6.7	N.D.	2.5	N.D.	3.43	−17.86	
S9-4	210	50	0.735	0.07	0.01 M citrate	7.0	N.D.	9.5	N.D.	5.28	−17.66	
S10-1	570		0.577	0.065	10^{-6} M EDTA	5.3	N.D.	2.17	N.D.	4.53	−17.66	
S10-2	170		0.577	0.07	10^{-5} M EDTA	5.43	N.D.	1.51	N.D.	4	−17.68	
S10-3	240		0.577	0.07	10^{-4} M EDTA	5.5	N.D.	5.25	N.D.	5.25	−17.56	
S10-4	210		0.577	0.068	10^{-3} M EDTA	5.6	N.D.	12.7	N.D.	12.4	−17.20	
S10-5	210	61	0.577	0.068	0.01 M EDTA	5.6	N.D.	N.D.	N.D.	N.D.	N.D.	
S11-1	570		0.55	0.076	0.1 mg/L alginate	5.19	No st.state	2.10	N.D.	3.1	−17.73	
S11-2	170		0.55	0.075	2.0 mg/L alginate	5.32	N.D.	1.78	N.D.	2.6	−17.81	
S11-4	210	45	0.55	0.075	100 mg/L alginate	5.42	N.D.	1.95	N.D.	2.00	−17.93	
S12-1	528		0.85	0.07	10^{-6} PO_4	5.86	0.9	2.42	<D.L.	3.58	−17.89	
S12-2	240		0.85	0.07	10^{-5} PO_4	6.01	0.8	2.44	<D.L.	3.27	−17.93	
S12-3	264		0.85	0.07	0.0001 M PO_4	5.83	0.7	2	<D.L.	3.45	−17.90	
S12-4	288		0.85	0.07	0.001 M PO_4	6.39	N.D.	1.7	<D.L.	2.03	−18.13	
S12-5	288		0.85	0.07	0.01 M PO_4	6.49	N.D.	1.92	0.86	N.D.		−18.09
S12-6	369	45	0.85	0.07	0.03 M PO_4	6.34	1	No st.state	0.56	N.D.		−18.27
S13-1	530		0.85	0.07	10^{-6} glucuronic	5.91	0.8	1.9	<D.L.	3.2	−17.94	
S13-2	240		0.85	0.07	10^{-5} glucuronic	5.85	N.D.	1.82	<D.L.	3.1	−17.96	
S13-3	260		0.85	0.07	0.0001 M glucuronic	5.81	0.7	1.68	<D.L.	2.8	−18.01	
S13-4	290		0.85	0.07	0.001 M glucuronic	6.00	N.D.	1.71	<D.L.	1.8	−18.20	
S13-5	290		0.85	0.07	0.01 M glucuronic	6.06	0.6	1.42	0.23	1.03	−18.45	−18.66
S13-6	370	49	0.85	0.07	0.03 M glucuronic	6.36	1.2	No st.state	0.35	0.83	−18.56	−18.48
S14-1	530		0.85	0.07	10^{-6} M 3,4-DHBA	5.95	N.D.	1.8	<D.L.	2.9	−17.99	
S14-2	240		0.85	0.07	10^{-5} M 3,4-DHBA	5.83	0.7	1.67	<D.L.	3.1	−17.96	
S14-3	260		0.85	0.07	0.0001 M 3,4-DHBA	5.82	0.7	1.63	0.16	2.78	−18.02	
S14-4	290		0.85	0.07	0.001 M 3,4-DHBA	5.88	0.5	1.54	0.656	1.78	−18.21	−18.21
S14-5	290		0.85	0.07	0.01 M 3,4-DHBA	6.04	0.6	1.41	2.3	2.45	−18.07	−17.76
S14-6	370	46	0.85	0.07	0.03 M 3,4-DHBA	6.74	2	3.7	2.66	6.1	−17.68	−17.60
S15-1	530		0.85	0.055	10^{-6} M glucosamine	6.25	0.7	2.07	<D.L.	4.05	−17.96	
S15-2	240		0.85	0.055	10^{-5} M glucosamine	6.05	0.53	1.97	<D.L.	3.9	−17.97	
S15-3	260		0.85	0.055	10^{-4} M glucosamine	6.11	0.8	1.93	<D.L.	3.2	−18.07	
S15-4	290		0.85	0.055	0.001 M glucosamine	6.16	0.7	1.74	0.29	2.15	−18.26	−18.71
S15-5	290		0.85	0.055	0.01 M glucosamine	6.37	0.95	1.7	1.71	2.09	−18.28	−17.94

Table 1 (*continued*)

Exp. Nos.	Duration, h	SSA final, m^2/g	Mass, g	Flow rate, ml/min	Composition	pH	[Ca], μM	[Mg], μM	[Al], μM	[Si], μM	$\log R_{Si}$	$\log R_{Al}$
S15-6	370	44	0.85	0.055	0.03 M glucosamine	6.56	No st.state	No st.state	2.52	No st.state	N.D.	−17.79
S16-1	528		0.85	0.06	10^{-6} M gluconate	6.16	1.1	2.47	<D.L.	4.50	−17.86	
S16-2	240		0.85	0.06	10^{-5} M gluconate	5.88	1	2.43	<D.L.	4.28	−17.90	
S16-3	264		0.85	0.06	0.0001 M gluconate	5.58	1.1	2.35	<D.L.	3.70	−17.91	
S16-4	290		0.85	0.06	0.001 M gluconate	5.48	0.8	2.27	<D.L.	3.52	−17.95	
S16-5	290		0.85	0.06	0.01 M gluconate	5.26	1.1	2.43	<D.L.	3.33	−18.00	
S16-6	370	53	0.85	0.06	0.03 M gluconate	6.50	No st.state	No st.state	<D.L.	2.10	−18.19	

The units of R are $mol/cm^2/s$. Background electrolyte is 0.01 M NaCl. pH is adjusted by HCl/NaOH addition. N.D. = not determined. D.L. = detection limit. All experiments except S7 and S8 are CO_2-free. Initial SSA is equal to 48 ± 4.8 m^2/g.

steady-state rate constants given in Table 1 are 15–20% and are dominated by the uncertainty on BET surface area measurements (±10%) and the standard deviation on average Si concentration at steady-state (±10% and ±15%, respectively). Uncertainties on Mg release are twice as large because steady-state with respect to Mg was not always achieved. In many experiments, rigorous analyses of Ca were not possible due to its very low concentrations.

Reacting fluids were comprised of deionized degassed H_2O, Merck reagent grade HCl, NaOH, $NaHCO_3$, Na_2CO_3, and NaCl. Experimental conditions for all dissolution experiments are listed in Table 1. Most experiments were performed at an ionic strength of 0.01 M maintained by a mixture of NaCl, HCl, and NaOH. In CO_2-free experiments, fresh input solution was purged of CO_2 by bubbling with pure nitrogen for 10–12 h; this bubbling was repeated once every two days during long-term dissolution experiments. Regular control of alkalinity and pH in inlet solutions for CO_2-free experiments did not reveal any detectable dissolution of atmospheric CO_2 via diffusion through polyethylene walls of the container in the course of experiments. Investigated inorganic and organic ligands were in the form of sodium salts or pure acids of analytical grade purchased from Fluka and Aldrich. All solutions were prepared from 18 MΩ ultrapure water (MilliQ Plus system) having a blank of dissolved organic carbon <0.05 ppm.

2.3. Solution analysis

All output solutions were analyzed for magnesium ($[Mg]_{tot}$), silica ($[SiO_2(aq)]_{tot}$), calcium ($[Ca]_{tot}$), and pH as a function of time. NBS buffers (pH = 4.008, 6.865, and 9.180 at 25 °C) were used for calibration of a combination pH-electrode (Schott Geräte H62). Precision of pH measurement was ±0.01 U. Alkalinity was determined following a standard HCl titration procedure with an uncertainty of ±1% and a detection limit of 5×10^{-5} M. Magnesium and calcium concentrations were measured by flame atomic absorption spectroscopy (Perkin-Elmer 5000PC) with an uncertainty of 1% and a detection limit of 1×10^{-7} and 3×10^{-7} M, respectively. Total silica concentration was determined using Technicon automatic analyzer by the molybdate blue method (Koroleff, 1976) with an uncertainty of 2% and a detection limit of 3×10^{-7} M. For several selected runs, analysis of dissolved aluminum was performed using atomic absorption with graphite furnace (Perkin-Elmer 5000PC) with an uncertainty of 5% and a detection limit of 3 nM. The concentration of organic ligands was measured as total dissolved organic carbon using a TOC Shimadzu 5000 analyzer with an uncertainty of 5% and a detection limit of 0.2 mg C_{org}/L.

Homogeneous solution equilibria were calculated for each solution composition using the MINTEQA2 code and MINTEQA2 thermodynamic database (Allison et al., 1991). The activity coefficients of free ions and charged complexes were calculated using the Davies equation which is standard in MINTEQA2. In the absence of a specific K_{eq} value for smectite sample SWy-2, the solubility constant of the MINTEQA2 thermodynamic database for Mg-endmember smectite ($Mg_{0.48}Fe_{0.22}Al_{1.71}Si_{3.81}O_{10}(OH)_2$, $\log K = -2.67$) was used in the calculation, consistent with those of SWy-1 used by Amram and Ganor (2005) and Metz et al. (2005a). Besides, additional calculations of saturation degree were performed with respect to (1) Na–montmorillonite $Na_{0.35}Mg_{0.35}Al_{1.65}Si_4O_{10}(OH)_2$ (Wilson et al., 2006), and (2) three different smectites (Ca, H, Na, K, and Na–montmorillonites) of the PHREEQC and EQ3NR (Wolery, 1983) database. Stability constants for Mg^{2+}(aq) and Ca^{2+}(aq) complexation with organic ligands were taken from the Critical Database (Martell et al., 1997).

2.4. Solid phase preparation for the analyses

At the end of an experimental run the reactors were opened. Smectite particles in the form of gel were collected from the dialysis bag and washed carefully twice with 150 ml of DI water. After washing the material, the smectite was divided in two parts. One part was used to prepare the XRD slides. For this, the smectite was resuspended five times for 1 min in an ultrasonic bath in 150 ml of 1 M $SrCl_2$

solution. Saturation with Sr^{2+} was used to ensure the presence of two water layers in the expandable layers under XRD data collection conditions. To promote complete cation exchange, the suspensions were stored after the ultrasonic treatment for 4 h at 50 °C. After this procedure the sample was washed five times with 150 ml of DI water. The second part of the sample was freeze dried for SEM-EDX observations, microwave digestion, XPS measurements, Infra-red, and SSA analysis.

2.5. X-ray photoelectron spectroscopy (XPS)

XPS was employed to monitor the fine changes in surface elemental ratio of the samples subjected to dissolution experiments and to verify the stoichiometry of the most surficial (~60–80 Å) layer. XPS analyses were performed using a Physical Electronics Inc. PHI 5600ci spectrometer equipped with a hemispherical capacitor analyzer and multichannel detector. Si 2s, Al 2p, and Mg 2s elemental lines were recorded by Al K_a X-ray excitation (1486.6 eV) with a source power of 200 W, source—sample distance of 10 mm and source—analyzer angle of 54°. The angle between sample surface normal and analyzer was 45°. Atomic concentrations were calculated from peak areas of elemental lines after Shirley background subtraction, by use of sensitivity factors and the analyzer transmission function was determined at the same acquisition parameters. Calibration of the Si, Al, and Mg analyses was performed using synthesized SiO_2, Al_2O_3, and $MgAlO_4$ samples. The SiO_2 (30 nm SiO_2 layer on silicon wafer), Al_2O_3 (sapphire single crystal, TBC-Kelpin Co., Neuhausen), and $MgAlO_4$ (99.985% $MgAlO_4$ powder, Alfa Aesar) samples were purified with ethanol and afterwards sputtered with Ar ions for 10–80 s. Based on the measurements of the ultra-pure solids, the PHI Multipak sensitivity factors were refined for the Al K_a X-ray excitation. The detection limit of the Si, Al, and Mg analyses is 0.5 mol%.

2.6. Microwave digestion

The elemental composition of the initial and the reacted smectite was determined following digestion with analytical grade aqua regia and boric acid in a microwave oven (Sawhney and Stilwell, 1994). The Na content was analysed by flame emission spectrometry. All other elements, including Si, Al, Fe, and Mg were determined by atomic adsorption spectrometry. Because the amount of reacted clays was limited no replicates were made.

2.7. Infra-red spectroscopy

IR spectroscopy was employed to follow the changes of water composition after the reaction and to assess the adsorbed organic ligands on the surface. The IR spectra were recorded with a Bruker IFS66/S spectrometer over the range 4000–400 cm^{-1} (optical resolution, 2 cm^{-1}). The pellets were prepared by diluting 1 mg of sample in 100 mg of KBr. The contribution of atmospheric water was always subtracted from the spectra.

2.8. X-ray diffraction

The evolution of clay mineral structure and the formation of secondary phases were monitored by XRD. Oriented slides were prepared by pipetting a slurry of Sr-saturated samples on a glass slide and drying it at room temperature for a few hours to obtain an air-dried preparation. Ethylene glycol solvation was achieved by exposing the oriented clay slides to ethylene glycol vapor at 60 °C for 12 h. XRD scans were recorded on a Bruker D5000 diffractometer (Cu radiation at 40 kV and 40 mA). The measuring range was from 2° to 50°2θ with a step size of 0.04° and 6 s counting time. The divergence slit, the two Soller slits, the antiscatter slit, and the resolution slit were 0.5°, 2.3°, 2.3°, 0.5°, and 0.06°, respectively.

2.9. Scanning electron microscopy

Scanning electron microscopy (SEM) was used to observe the morphological changes in smectite particles in the course of dissolution reaction and to characterize the material whose amount was insufficient for structural XRD analysis. The SEM photographs were obtained using a CanScan FE44 SEM equipped with a Noran EDS unit. SEM-EDS measurements were performed at an accelerating voltage of 20 kV and a current of 1 nA. ZAF corrections were made using the Noran evaluation software for the CamScan FE44 instrument. Raw powders of all samples and powders after pretreatment and after dissolution experiments of smectites SWy-2 were examined. Generally, average results of 15 SEM-EDS replicate measurements per sample are used for the Al/Si and Mg/Si ratio calculations. A detailed description of the calibration procedure can be found in Metz et al. (2005a).

2.10. Specific surface area measurements

Specific surface area (SSA) was determined by measurement of N_2 isotherm having nine points of adsorption at partial pressure ranging from 0.01 to 0.3 p/p_0 at 77 K using a Quantachrome Autosorb1-MP instrument. The cross section of adsorbed N_2 was assumed to be 0.162 nm^2. Prior to adsorption the samples were degassed in vacuum at 110 °C overnight. SSA was calculated with the BET method (Brunauer et al., 1932). The accuracy of the BET technique was ±10%.

3. Results and discussion

3.1. Solid phase characterization

All reacted solid with solutions of prescribed composition (Table 1) were characterized by XRD, Infra-red spectroscopy, XPS, chemical analysis after microwave

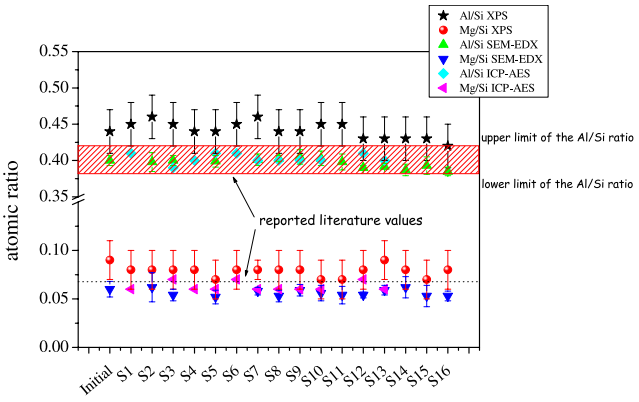

Fig. 1. Molar Al/Si and Mg/Si on the surface and in the bulk of initial and reacted smectites determined by XPS, SEM-EDX and total chemical analysis. The literature data are from Stucki et al. (1984) and Mermut and Cano (2001). The list of experiments is given in Table 1.

digestion, and SEM-EDX observations. The total amount of smectite dissolved during any single experiment was less than 5% of the initial solid. All XRD patterns were identical and very close to the initial non-reacted material. In none of them were secondary minerals detected. No decrease in intensity of the 00l reflections nor a peak broadening was observed (not shown).

The molar Al/Si and Mg/Si ratios determined by SEM-EDX and by chemical analysis after microwave digestion were close to the initial (unreacted) sample SWy-2, in good agreement with the literature data (Stucki et al., 1984; Mermut and Cano, 2001), Fig. 1. The ratios determined by XPS were always slightly higher.

SEM images did not reveal the presence of secondary minerals. SEM images of initial and post-experiment smectite were indistinguishable at the resolution of scanning electron microscope used in this study (Fig. 2A–D).

Transmission FT-IR and Diffuse Reflectance (DRIFT) spectra of reacted powders did not reveal any significant changes in the intensity and band positions of characteristic vibration peaks of smectite and the adsorbed ligands could not be resolved within the presicion of technique (not shown). The BET surface area of post-experiment smectite varied between 43 and 54 m^2/g (Table 1). These values are within the uncertainty of the measurement of initial value (48 ± 5 m^2/g). Only in the experiment S10-5 (210 h in 0.01 M EDTA) the BET surface area increased to 61 m^2/g, likely due to expanding the surface layers and the increase of the interfoliar space and microporosity or disintegration of grains. Such an increase in specific surface areas has been reported in recent studies of smectite reactivity (Metz et al., 2005b).

3.2. Steady-state attainment and the stoichiometry of dissolution reaction

Examples of the variation of measured outlet Si, Mg, Ca, and Al concentrations during smectite SWy-2 dissolution as a function of elapsed time are illustrated in the Appendix A. Steady-state for Si was typically reached after 200–500 h depending on the flow rate. For each experiment, at least five data points at steady-state conditions were collected. It can be seen that within the uncertainty of ±15–20%, outlet Si and Al concentrations remain constant once the steady-state is attained. Note that for many experiments, steady-state with respect to Mg was not achieved and low Ca concentration prevented its quantification.

Results of 65 steady-state dissolution experiments performed in CO_2-free and CO_2-bearing solutions at pH from 1 to 12 and ionic strength from 0.01 to 0.1 M are listed in Table 1. Included in this table are reacting mass of solid, fluid flow rates, inlet fluid composition (or blank concentrations), outlet fluid pH, $[Mg]_{tot}$, $[SiO_2(aq)]_{tot}$, $[Ca]_{tot}$, and $[Al]_{tot}$ (for some experiments), and steady-state smectite dissolution rates computed using Eq. (1). For all experiments listed in Table 1, the outlet solutions were strongly undersaturated with respect to smectite, brucite, quartz and amorphous silica, and kaolinite (saturation indices are below 0.02). For some experiments performed in alkaline solutions (i.e., Nos. S3, S6-1, S8-4), supersaturation with respect to chrysotile, talc, and brucite was found. All outlet solutions were strongly undersaturated with respect to four types of smectite whose solubility products were available (see Section 2.3): the saturation indices were below 10^{-3} corresponding to $\Delta G_r = -20 \pm 10$ kcal/mol. For assessing $a_{Al^{3+}}$ in these calculations, we used both measured $[Al]_{outlet}$ and calculated $[Al]_{outlet}$ assuming (i) stoichiometric Al vs. Si release or (ii) equilibrium with gibbsite. Accordingly, stoichiometric Fe(III) vs. Si release and calculated goethite solubility as a function of pH were used as proxies for $a_{Fe^{3+}}$. At these degrees of saturation, the dissolution is not affected by ΔG_r as it is the case for kaolinite (Nagy et al., 1991; Cama and Ganor, 2006).

The relative stoichiometry of Al, Mg, and Si as a function of pH can be assessed from the comparison of elemental ratios in the outlet fluid and in mineral structure as depicted in Fig. 3. The dissolution is strongly non-stoichiometric in acid to weakly alkaline solution with $R_{Al} < R_{Si} < R_{Mg}$ (Fig. 4). In basic solutions, at pH ~ 10.5, aluminum, silica, and magnesium-release-based rates are very close. At $4 < pH \leqslant 10$, Al concentration in solution could not be resolved even on nanomolar level using GF-AAS and the outlet Al/Si ratio was much lower than that of the dissolving smectite. This observation is consistent with results of solute speciation calculations showing that these solutions are close to equilibrium or supersaturated with gibbsite. The quantity of thus precipitating gibbsite was calculated from smectite stoichiometry and $[Si]_{outlet}$, experiment duration and the flow rate and was found to vary from 0.1% to 1% of the initial mass of smectite. These quantities could not be detected by microscopic and spectroscopic techniques used in our study. At pH below 4 in solutions undersaturated with respect to Al hydroxides, the Al/Si ratio in the outlet fluid is still lower than that in the solid. This is consistent with results of Zysset and

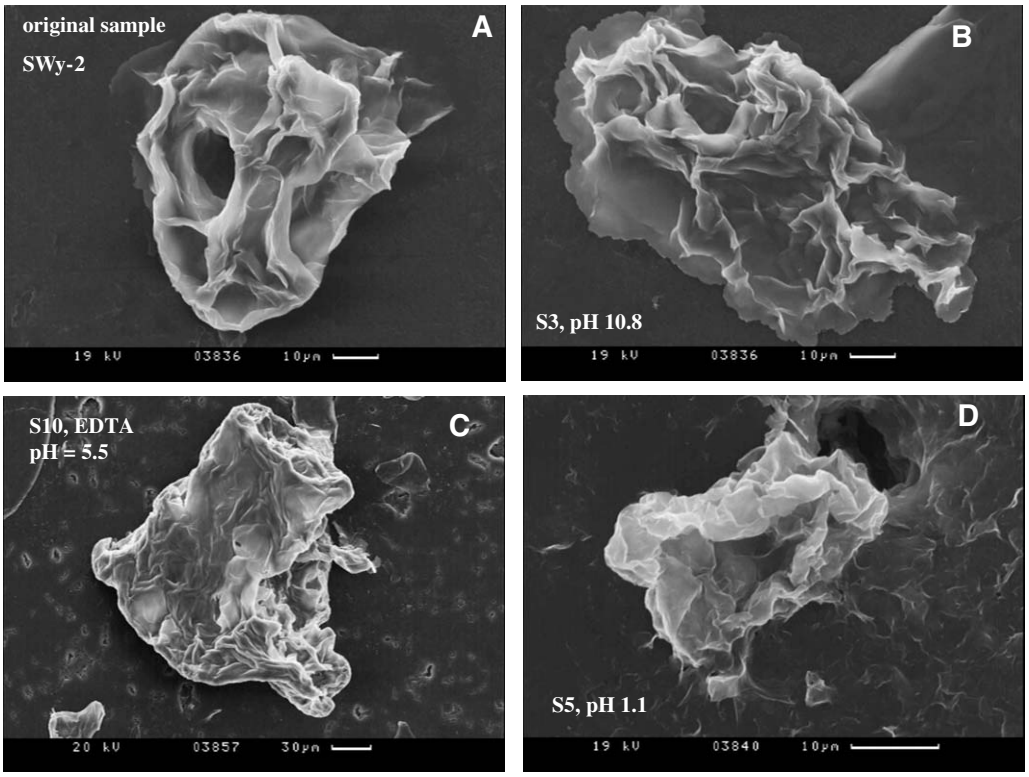

Fig. 2. SEM photomicrographs showing the smectite aggregates used in this study: (A) initial grains, (B) after dissolution at pH 10.8–10.5 during 1222 h, (C) after dissolution at pH 5.5 in the presence of 0.001 M EDTA during 210 h, and (D) after dissolution at pH 1.1 during 615 h.

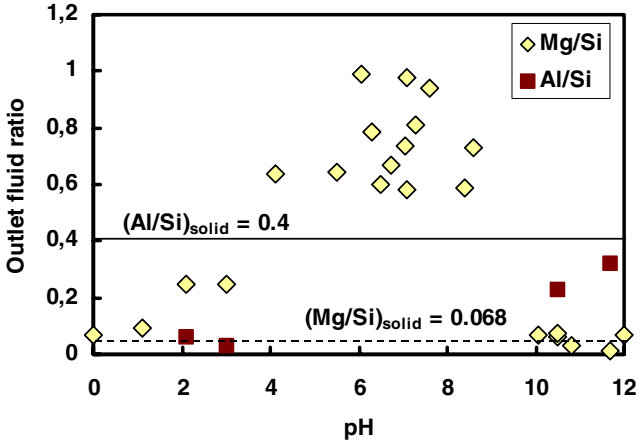

Fig. 3. Molar Mg/Si (diamonds) and Al:Si (squares) ratio in the outlet fluid after 1000–1500 h of reaction as a function of pH. Stochiometric dissolution is observed only in strongly acidic and alkaline solutions. Adsorption of Al on the interlayer positions at pH < 4.5 and proton-octahedral magnesium exchange at 2 < pH < 10 are suggested to explain this non-stoichiometry (see Section 3.2).

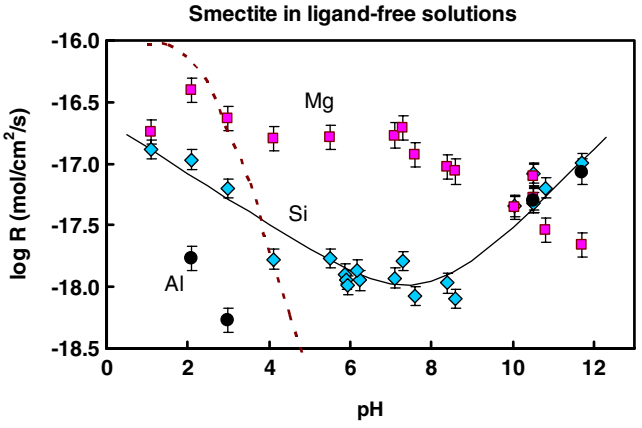

Fig. 4. Summary of smectite dissolution at 25 °C as a function of pH in CO_2-free and CO_2-bearing solutions. Diamonds, Si-based rates; squares, non-stoichiometric Mg release; circles, Al-based rates. The solid line represents the fit of experimental data to Eq. (3) (see explanation in the text). Thick dash line corresponds to Amram and Ganor (2005) data.

Schindler (1996), who reported, for K–montmorillonite at 25 °C and 1.5 < pH ⩽ 4 in 0.03 M KCl, the solution ratio Al/Si being significantly lower than that of the solid phase. These authors attributed this feature to the adsorption of dissolved Al(III) on cation exchanger (interlayer) sites as also reported by Charlet et al. (1993). It is possible that similar reaction occurs in our rather diluted (0.01 M NaCl) solutions reacting with Na–montmorillonite that provides apparent Al/Si non-stoichiometry in acidic solutions.

Magnesium is released stoichiometrically with silica only at pH = 1.1 and pH = 10.5–10.8. (exp # S5-2 and S8-3, S8-4, respectively, Table 1). At pH around 11, a preferential retention of Mg in the solid is observed (exp No. S6-1) which can be explained by supersaturation with respect to brucite and chrysotile as calculated using MINTEQA2. A rather surprising result is the non-stoichiometric Mg vs.

Si release after 1000–1500 h in all experiments having pH below 10.5–11. This cannot be explained by precipitation of any secondary Mg-bearing silicate phases because outlet solutions were undersaturated with respect to any such solid phase. While the ion-exchange processes responsible for rapid release of loosely bound Ca of the interlayer sites are very well known (Ferrage et al., 2005; Metz et al., 2005a), non-stoichiometric Mg release cannot be explained by removal of exchangeable ions since there is no Mg in the interlayer positions of the SWy-2 Na–montmorillonite. Therefore, we evoke the cation–proton exchange of the octahedral-layer structural component in the way it is observed for feldspars (Casey et al., 1988; Blum and Stillings, 1995), pyroxenes (Casey et al., 1993b; Oelkers and Schott, 2001) and orthosilicates (Wogelius and Walther, 1991; Pokrovsky and Schott, 2000a,b). Note that this incongruent dissolution cannot be detected by spectroscopic techniques used in this study as only 0.1–1% of initial Mg is removed due to this structural cation–proton exchange reaction. As such, our Mg-based rates do not correspond to the steady-state mineral dissolution and smectite reactivity will be quantified in terms of silica release.

3.3. Effect of pH on smectite dissolution rates

Smectite steady-state dissolution rates measured at 25 °C in CO_2-free and CO_2-bearing solutions at ionic strengths ranging from 0.01 to 0.1 M are depicted as a function of pH in Fig. 4. For comparison, SAz-1 dissolution rates determined by Amram and Ganor (2005) at $I = 0.32$ M are shown in the same figure. It can be seen that the rates measured in the present study are not consistent with the stoichiometric adsorption of protons following the Langmuir isotherm (Amram and Ganor, 2005), therefore, an empirical expression for Si-release rates can be used (Kohler et al., 2003). This expression is generated by adopting an empirical rate equation describing the isothermal variation of rates with pH of the form (cf. Murphy and Helgeson, 1987; Blum and Lasaga, 1988; Wieland and Stumm, 1992; Zysset and Schindler, 1996)

$$R = k_{\mathrm{H}} \cdot a_{\mathrm{H^+}}^{n\mathrm{H}} + k_{\mathrm{H_2O}} + k_{\mathrm{OH}} \cdot a_{\mathrm{OH^-}}^{n\mathrm{OH}} \quad (2)$$

Where k_{H}, k_{OH}, and $k_{\mathrm{H_2O}}$ refer to rate constants, a_{i} signifies the activity of subscribed aqueous species, and n_{H} and n_{OH} stand for the apparent order of the dissolution reaction with respect to H^+ and OH^-, respectively. Apparent smectite dissolution rates obtained in the present study were regressed using Eq. (2) to obtain k_{H}, k_{OH}, $k_{\mathrm{H_2O}}$, n_{H}, and n_{OH}. The results of this regression yield the following empirical expressions describing the apparent SWy-2 smectite long-term, steady-state dissolution rates [mol/cm^2/s] for the main constituent of the mineral:

$$R_{\mathrm{Si}} = 2.2 \cdot 10^{-17} \cdot a_{\mathrm{H^+}}^{0.21} + 1.0 \cdot 10^{-20} + 6 \cdot 10^{-17} \cdot a_{\mathrm{OH^-}}^{0.33} \quad (3)$$

We observe an invariability of Ca release vs. pH which implies that interlayer Ca cation exchange is pH independent at $2 \leqslant \mathrm{pH} \leqslant 8$ (not shown). Mg-based rates could not be assessed due to strong non-stoichiometry with respect to Si and the absence of true chemical steady-state (see Section 3.2). The degree to which Eq. (3) can describe the apparent smectite dissolution rate obtained in the present study can be gauged with the aid of Fig. 4, where the solid curve represents the result of regression calculation and the symbols correspond to measured rates. It can be seen that, within the experimental reproducibility of rate measurement (i.e., ±0.2–0.3 log R units which is typical for such slow-dissolving minerals attaining the steady-state over long period of time, see Amram and Ganor, 2005), Eq. (3) adequately reproduces apparent smectite dissolution rates at $1 < \mathrm{pH} < 12$. The reaction orders with respect to $a_{\mathrm{H^+}}$ and $a_{\mathrm{OH^-}}$ for Si-release rates observed in the present study (~0.2 and ~0.3, respectively) are slightly lower than the values reported for other clay minerals (see compilation and discussion in Kohler et al., 2003), although the order $n_{\mathrm{H}} < n_{\mathrm{OH}}$ is met and the absolute values of Si-based rates are comparable, within a half an order of magnitude, with those of Zysset and Schindler (1996) and Amram and Ganor (2005) in acidic solutions, and Huertas et al. (2001) in neutral solutions. Quantitative comparison of our data with those of Metz et al. (2005a,b) and Amram and Ganor (2005) is not straightforward because of different methods of rate normalization: per gram of solid in those studies and per cm^2 in this work. It has been widely argued that the BET surface area cannot serve as a proxy for the reactive surface area (Metz et al., 2005b), however, for consistency with earlier studies and because the BET surface area did not vary significantly in the course of dissolution reaction (Table 1), we used surface area rate normalization in this work.

3.4. Effect of ligands on smectite dissolution rates

We tested several families of organic compounds that represent both individual organic acids identified in soil solutions and groundwaters and chemical analogs of microbial exometabolites, functional groups of cell surface envelopes and various specific binding ligands. For this, mono and di(tri)carboxylic acids (acetate, gluconate, oxalate, and citrate), chelates (EDTA) and most important inorganic ligands (phosphate and carbonate) were retained. Aromatic compounds used in the present study can be considered as analogs of aromatic groups of natural polymers or extracellular microbial chelates, 3,4-dihydroxybenzoic acid (3,4-DHBA, Rogers and Bennet, 2004). Apart of these simple synthetic compounds, natural ligands such as alginate from brown algae, glucosamine, and glucuronic acid as analogs of microbial extracellular polysaccharides and bacterial peptidoglycan were also tested with respect to their effect on smectite dissolution.

Ligands investigated in this study can be distributed among two groups according to their influence on dissolution rates. The addition of "catalysts" at neutral pH leads to an increase of the dissolution rate with the following effectiveness: EDTA > 3,4-DHBA > citrate ⩾ oxalate.

This is illustrated in Fig. 5 where smectite Si-based dissolution rates are plotted as a function of ligand concentration in solution. The addition of "inhibitors" leads to a decrease of the dissolution rate with the following effectiveness: glucuronate $\geqslant$ phosphate $\geqslant$ acetate $>$ glucosamine $>$ gluconate $\sim$ alginate. This classification takes into account relative effect of each ligand depending on ligands concentration. Increasing of bicarbonate (5×10^{-4} to 0.01 M) and carbonate concentrations (5×10^{-4} to 0.0033 M) has no effect on smectite dissolution within the uncertainties of rate measurements. Indeed, the rates measured in the presence of HCO_3^- and CO_3^{2-} match those calculated using Eq. (3) in ligand-free systems. All studied ligands only weakly affect Mg release up to $[Ligand]_{tot} < 0.01$ M and provoke the increase of Mg outlet concentration at $[Ligand]_{tot} > 0.01$ M (Fig. 6). In the presence of high concentrations of organic ligands, able to complex Al^{3+} in solution and thus to prevent the precipitation of secondary

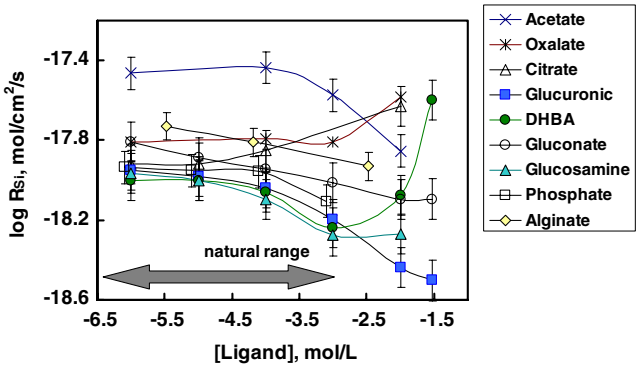

Fig. 5. Silica-release-based dissolution rates of smectite SWy-2 in organic-bearing solutions at 25 °C, $I = 0.01$ M and constant pH for each ligand (average pH $= 6.08 \pm 0.45$, see Tables 1 and 2). The symbols represent the experimental data and the solid lines are for guiding purposes. For acetate and oxalate it is postulated that ligand-free experiments rates are equivalent to 10^{-6} M oxalate or acetate since no effect is observed till 10^{-4} M.

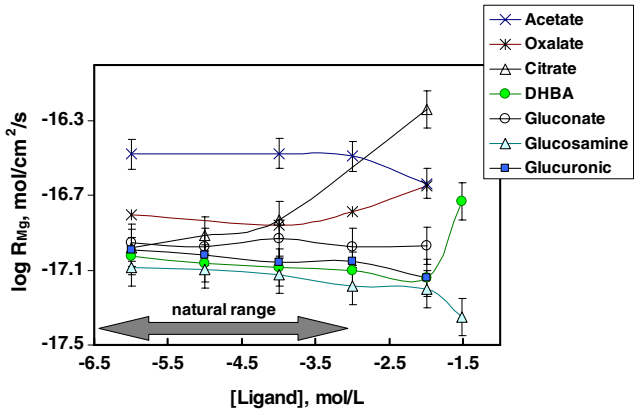

Fig. 6. Rates of non-stoichiometric magnesium release from SWy-2 smectite in organic-bearing solutions at 25 °C, $I = 0.01$ M and pH $= 6.08 \pm 0.45$. The symbols represent the experimental data and the solid lines are for guiding purposes.

Al-bearing phases, the Al-release-based rates (R_{Al}) were similar, within 0.2 log R units, to those of silica-release-based (R_{si}) as seen from comparison of runs S15-5; S14-4,5,6; S13-5, 6 (Table 1).

Only a few studies addressed the effect of complex-forming ligands, such as low-molecular-weight organic acids and fulvic acids, on the dissolution of phyllosilicates, Schnitzer and Kodama (1976) showed that the decomposition of mica is not significantly enhanced in the presence of fulvic acid. Complex-forming ligands (e.g., aspartic, citric, salicylic, tartaric, and tannic acids) promote the dissolution of clay minerals and change the stoichiometry of Al and Si release (Huang and Keller, 1971). Carroll-Webb and Walther (1988) reported that long-term dissolution of kaolinite was not affected by organic ligands such as phthalate, succinate, malonate, and TRIS whereas Cama and Ganor (2006) observed the effect of oxalate at $[Oxalate^{2-}] \geqslant 10^{-3}$ M.

The effect of ligands on smectite dissolution can be modeled conceptually as surface adsorption assuming the overall dissolution rate is the sum of all the different parallel dissolution reactions promoted at active centers (presumably, Mg–O–Si and/or Al–O–Si bonds) by various reactants/ligands which compete for available surface sites (Stumm, 1992). The effectiveness of ligands depends both on the nature of their functional groups, molecular structure and thermodynamic stability of the surface complexes they form. It is known that especially efficient are ligands whose functional groups contain two or more oxygen donors and which can form bi or multidentate mononuclear surface chelates (Stumm, 1992, 1997). In contrast, ligands forming bi or polynuclear complexes, that can bridge two or more metal centers at the mineral surface are known to retard dissolution.

At the experimental conditions of this study, most ligands were present in the form of -1 or -2 charged species (Table 2). The edges of the smectite particles are positively charged in solutions at pH below 7.5–8 (i.e., Stadler and Schindler, 1993; Huertas et al., 2001). Therefore, in the pH range used to study the ligand effect on smectite dissolution, the simplest surface reaction between positively charged surface groups ($\{>S^{x+}\}^*$, presumably, >Al–O^+–Si or $>AlOH_2^+$, Zysset and Schindler, 1996, or $>MgOH_2^+$ groups as for other Mg-bearing multiple oxides) and negatively charged ligands can be considered. According to this scheme, the rate of ligand-controlled dissolution is proportional to the concentration of the surface center–ligand complex $>S–L^{x-n}$ (S = Si, Al, and Mg) which can be deduced from the reaction (4a) stability constant:

$$>S^{x+} + L^{n-} => S–L^{x-n} + H_2O, K^*_{S–L} \quad (4a)$$

$$K^*_{S–L} = \frac{\{> S–L^{x-n}\}}{\{> S^{x+}\} \times [L^{n-}]} \quad (4b)$$

In the presence of a ligand at neutral pH, the smectite forward dissolution rate is thus the sum of H_2O- ($k^*_{H_2O}$) and ligand-controlled dissolution, similar to that of brucite

Table 2
Parameters of Eq. (8) for ligand-affected dissolution rate of smectite at constant pH

Ligand	pK_a	Speciation	pH	K^*_{S-L}	$k^{\#}_{Si}$	$k^{\#}_{L}$
Acetate	3.75	100% acetate$^-$	6.41	150 ± 50	$(3.4 \pm 0.1) \cdot 10^{-18}$	$(2.0 \pm 0.5) \cdot 10^{-20}$
Oxalate	1.25; 4.27	100% oxalate^{2-}	6.78	200 ± 50	$(1.53 \pm 0.05) \cdot 10^{-18}$	$(3.2 \pm 0.2) \cdot 10^{-18}$
Citrate	3.13; 4.76; 6.40	23% HCitr$^-$, 77% Citr^{2-}	6.63	500 ± 50	$(1.2 \pm 0.1) \cdot 10^{-18}$	$(2.5 \pm 0.1) \cdot 10^{-18}$
Gluconate	3.46	100% gluconate$^-$	5.81	200 ± 20	$(1.35 \pm 0.05) \cdot 10^{-18}$	$(6.5 \pm 0.5) \cdot 10^{-19}$
EDTA	2.0; 2.7; 6.3; 10.9	22% H_3EDTA-, 78% H_2EDTA^{2-}	5.46	1000 ± 100	$(1.93 \pm 0.05) \cdot 10^{-18}$	$(1.15 \pm 0.1) \cdot 10^{-17}$
Phosphate	2.15; 7.20; 12.38	11% HPO_4^{2-}, 89% $H_2PO_4^-$	6.15	700 ± 50	$(1.15 \pm 0.1) \cdot 10^{-18}$	$(1.0 \pm 0.2) \cdot 10^{-19}$
3,4-DHBA	4.5; 9.0	100% H-DHBA$^-$	6.04	75 ± 5	$(9.0 \pm 0.1) \cdot 10^{-19}$	$(2.9 \pm 0.2) \cdot 10^{-18}$
Glucuronate	(12.04)	100% glucuronate$^-$	6.00	600 ± 50	$(1.1 \pm 0.1) \cdot 10^{-18}$	$(2.7 \pm 0.2) \cdot 10^{-19}$
Glucosamine	7.58	100% glucosamine^o	6.25	500 ± 50	$(1.0 \pm 0.1) \cdot 10^{-18}$	$(4.2 \pm 0.3) \cdot 10^{-19}$
Alginate (30,000 g/mol)	3.46	100% alginate$^-$	5.32	150 ± 30	$(1.8 \pm 0.1) \cdot 10^{-18}$	$(1.0 \pm 0.5) \cdot 10^{-18}$

(Pokrovsky et al., 2005a) and dolomite (Pokrovsky and Schott, 2001):

$$R = k^*_{H_2O} + k_L \cdot \{> S\text{–}L^{x-n}\} \quad (5)$$

where k_L is the empirical kinetic constant pertinent to each ligand. Upon the adsorption of a ligand on the initial rate-controlling sites, their concentration decreases such that $k^*_{H_2O}$ Eq. (5) is less than k_{H_2O} Eq. (3). We will assume that at constant pH of our experiments, the ligand sorption on mineral surface follows a Langmurian adsorption isotherm with mass law conservation for the surface sites:

$$S_T = \{> S^{x+}\}^* + \{> S\text{–}L^{x-n}\} \quad (6)$$

where $\{>S^{x+}\}^*$ designates the rate-controlling surface sites, non-occupied by the ligand ($>AlOH_2^+$, $>SiOH^\circ$ or $>MgOH_2^+$). Note that such a macroscopic phenomenological approach allows to model the effect of rates without resolving the true molecular nature of ligand-surface sites complexes. Moreover, we assume the simplest mechanism of ligand-promoted dissolution when the dissolution rate is proportional to adsorbed ligand concentration as the small number of rate data points in our study does not allow testing other dependencies such as, for example, quadratic or protonated ligand effect (Cama and Ganor, 2006). Therefore, one can combine Eqs. (4b) and (6) to calculate the concentration of adsorbed ligand Eq. (7a) and rate-controlling surface sites, non-occupied by the ligand Eq. (7b), respectively:

$$\{> S\text{–}L^{x-n}\} = \frac{S_T \cdot K^*_{S-L} \cdot [L^{n-}]}{1 + K^*_{S-L} \cdot [L^{n-}]} \quad (7a)$$

$$\{> S^{x+}\}^* = S_T \cdot \left(1 - \frac{K^*_{S-L} \cdot [L^{n-}]}{1 + K^*_{S-L} \cdot [L^{n-}]}\right) \quad (7b)$$

Combining Eqs. (5) and (7a) provides:

$$R = k^*_{Si} \cdot \{> S^{x+}\}^* + k_L \cdot \frac{S_T \cdot K^*_{S-L} \cdot [L^{n-}]}{1 + K^*_{S-L} \cdot [L^{n-}]} \quad (8a)$$

and combination of Eqs. (8a) and (7b) yields:

$$R = k^{\#}_{Si} \cdot \left(1 - \frac{K^*_{S-L} \cdot [L^{n-}]}{1 + K^*_{S-L} \cdot [L^{n-}]}\right) + k^{\#}_{L} \cdot \frac{K^*_{S-L} \cdot [L^{n-}]}{1 + K^*_{S-L} \cdot [L^{n-}]} \quad (8b)$$

where the first term represents $k^*_{H_2O}$ in Eq. (5), and $k^{\#}_i = k_i \cdot S_T$ with $i =$ Si,L.

It has to be noted that in series of experiments with a given ligand, the pH slightly varies from one individual run to another (Table 1). Although these variations are within the uncertainties of the experiments, such conditions make the Eq. (8b) invalid. Therefore, in order to model the rates obtained at slightly different pH depending on different ligand concentrations, we re-calculated all rates with ligands to the same pH following the log R–pH dependence given by Eq. (3). This "reference" pH was choosing as the average pH for series with each ligand, the average value for all ligands being equal to 6.08 ± 0.45. Because all experiments with ligands were conducted in circum-neutral solutions where the rates are almost independent on pH, corrections for the rates after subtraction the effect of pH vary from 0.01 to 0.05 log R units.

Application of Eq. (8b) to model the experimental dependence of smectite dissolution on ligand concentration requires accurate values of K^*_{S-L} for the ligands investigated in this study. Such values were generated from the fitting of dissolution rate dependencies on aqueous ligand concentrations. The fitting procedure performed by "trial and error" consisted in assuming that the values of the equilibrium constants for ligands adsorption were the same as the corresponding values for Mg(Si)-ligand association reactions in aqueous solution (Schindler and Stumm, 1987). Note that for this fitting, the use of Al^{3+}–L^{n-} aqueous complexes as proxies for ligand adsorption on Al–O^+–Si sites was not possible: very high values for aqueous complex stability constants yielded physically unrealistic shapes of the log R–log [L] dependencies. The values of $k^{\#}_L$ were set first equal to $k^{\#}_{Si}$ assuming no inhibition or catalyses occurs. Then, the values of rate constants $k^{\#}_L$ were allowed to increase/decrease in order to fit the experimental dependence of dissolution rate on ligand concentration using Eq. (8b). The values of $k^{\#}_{Si}$ at a given pH for each ligand were determined for the lowest ligand concentration. When fitting was not possible with the selected value of K^*_{S-L}, it was allowed to vary within one order of magnitude from the initial settings. A $\leqslant$20% disagreement between measured and modeled Eq. (8b) rate values at each ligand concentration was taken as a criterion of goodness of fit. The final values of constants used in Eq. (8b) are listed in Table 2. The

uncertainties attached to these values correspond to the range of best fits obtained by varying the $k_L^{\#}$ and K_{S-L}^{*}. Note that arbitrary change in K_{S-L}^{*} or $k_L^{\#}$ values was not possible: for example, at any value of $k_L^{\#}$, the deviation of K_{S-L}^{*} by 1–2 orders of magnitude from the values used in this work, would force the calculated log R–log [L] curve to become fully inconsistent with the experimental data. The degree to which Eq. (8b) can be used to describe the effect of investigated ligands on smectite dissolution rate can be assessed in Fig. 7. The solid curves depicted in these figures were computed with Eq. (8b) using values of K_{S-L}^{*}, $k_L^{\#}$, and $k_{Si}^{\#}$ listed in Table 2. The close correspondence between the solid curves and the experimental data for a very broad range of a ligand's aqueous concentration demonstrates the validity of Eq. (8b). The only exception is 3,4-DHBA whose presence brings about a sigmoid dependence of R on [L] (Fig. 7), not reproduced by the model at [3,4-DHBA] equal to 0.001 and 0.01 M. It is possible, that due to high affinity of silica to aromatic compounds such as catechol (i.e., Pokrovski and Schott, 1998) and, presumably, DHBA, the adsorption of the latter occurs onto several independent surface sites such as >SiOH° and $>AlOH_2^+$,

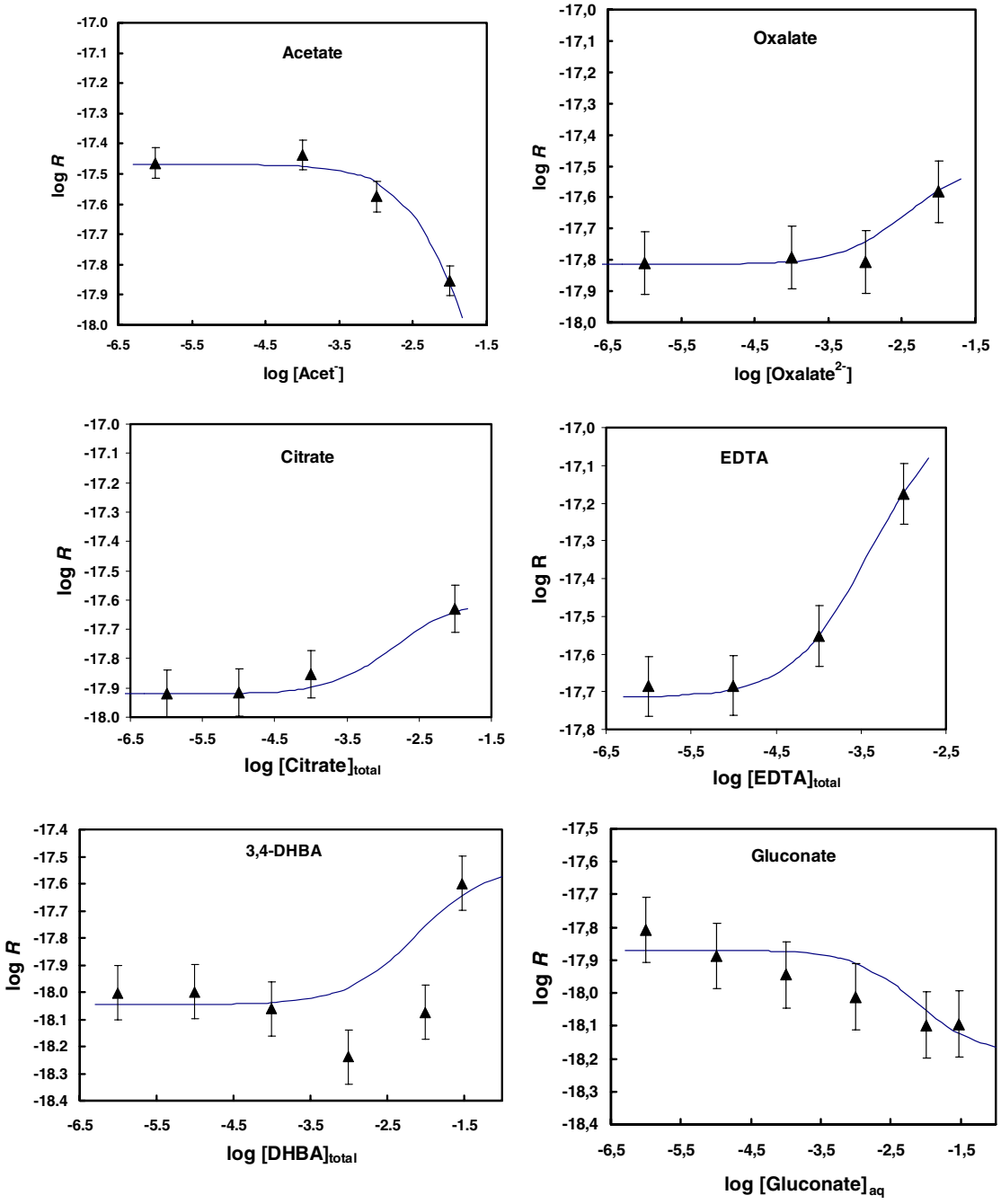

Fig. 7. Effect of added ligands on smectite Si-based steady-state dissolution rates. Triangles represent Si-release-based rates and the solid lines represent the fit to the data using Eq. (8) with parameters listed in Table 2.

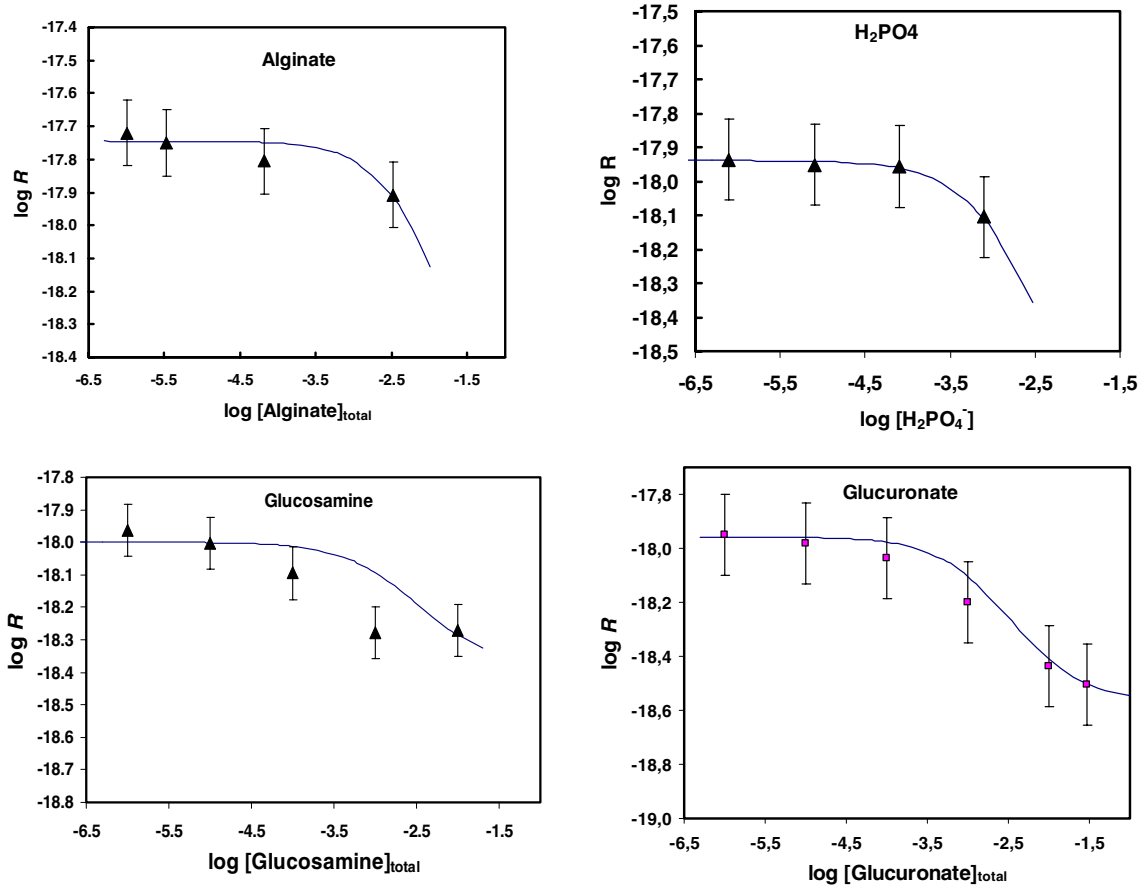

Fig 7. (*continued*)

including basal planes and not only edges, and thus Eq. (8b) becomes invalid.

The relative inhibiting/catalyzing effect of ligands on smectite dissolution can be understood following the analogy with ligand effect and surface structure on simple oxides and other clay minerals (Nagy, 1995; Stumm, 1997; Pokrovsky et al., 2005a). It is known that the ligands bind to the surface with increasing strength in the order: carbonate $<$ acetate $\ll$ oxalate $\leqslant$ citrate (Nagy, 1995) and this is consistent with the sequence of ligand effect observed in the present study. EDTA and aromatic compounds (3,4-DHBA) both of which are likely to form very stable five-membered chelate rings with surface Al and Mg ions, present the strongest catalyzing effect on smectite dissolution. The inhibiting effect of polysaccharides (analogs of bacterial exudates and cell envelopes) corroborates the previous results of Welch and co-authors (Welch and Vandevivere, 1994; Welch et al., 1999) and Pokrovsky et al. (2004) for ligand-affected aluminosilicate and wollastonite dissolution, respectively; it has been established that long chain acid polysaccharides such as pectin, algae exudates, glucuronic, and alginic acid inhibit the dissolution rate of silicates because they bind 'irreversibly' to multiple sites on the mineral surface thus forming multinuclear complexes. However, further detailed structural experimental (AFM) and theoretical (molecular modeling) studies are necessary to better resolve the interaction of organic ligands with mineral surfaces (i.e., Becker et al., 2005).

3.5. Implications for smectite weathering in natural environment

The rates of Si release from smectite SWy-2 measured in this study correspond to steady-state condition of dissolution reaction; however, strong non-stoichiometry between Mg, Al, and Si was observed. While for Al it could be related to secondary minerals formation and re-adsorption on the interlayer sites, the Mg/Si non-stoichiometry reflects non-steady state conditions corresponding to the exchange between protons and structural Mg. Recently, it has been suggested that continuous decrease in dissolution rates over long period of time (100–200 days) occurs during laboratory experiments of clay minerals dissolution (Kohler et al., 2005). The reason for this decrease is that the edges of clay minerals dissolve faster than the basal planes (Wieland and Stumm, 1992; Ganor et al., 1995; Bosbach et al., 2000; Bickmore et al., 2001). As a result, the dissolution tends to change clay morphology decreasing the percentage of reactive edge sites. Although we did not detect any visible change of smectite morphology during dissolution experiments, the non-stoichiometric release of major mineral constituents during 200–1000 h reaction did occur.

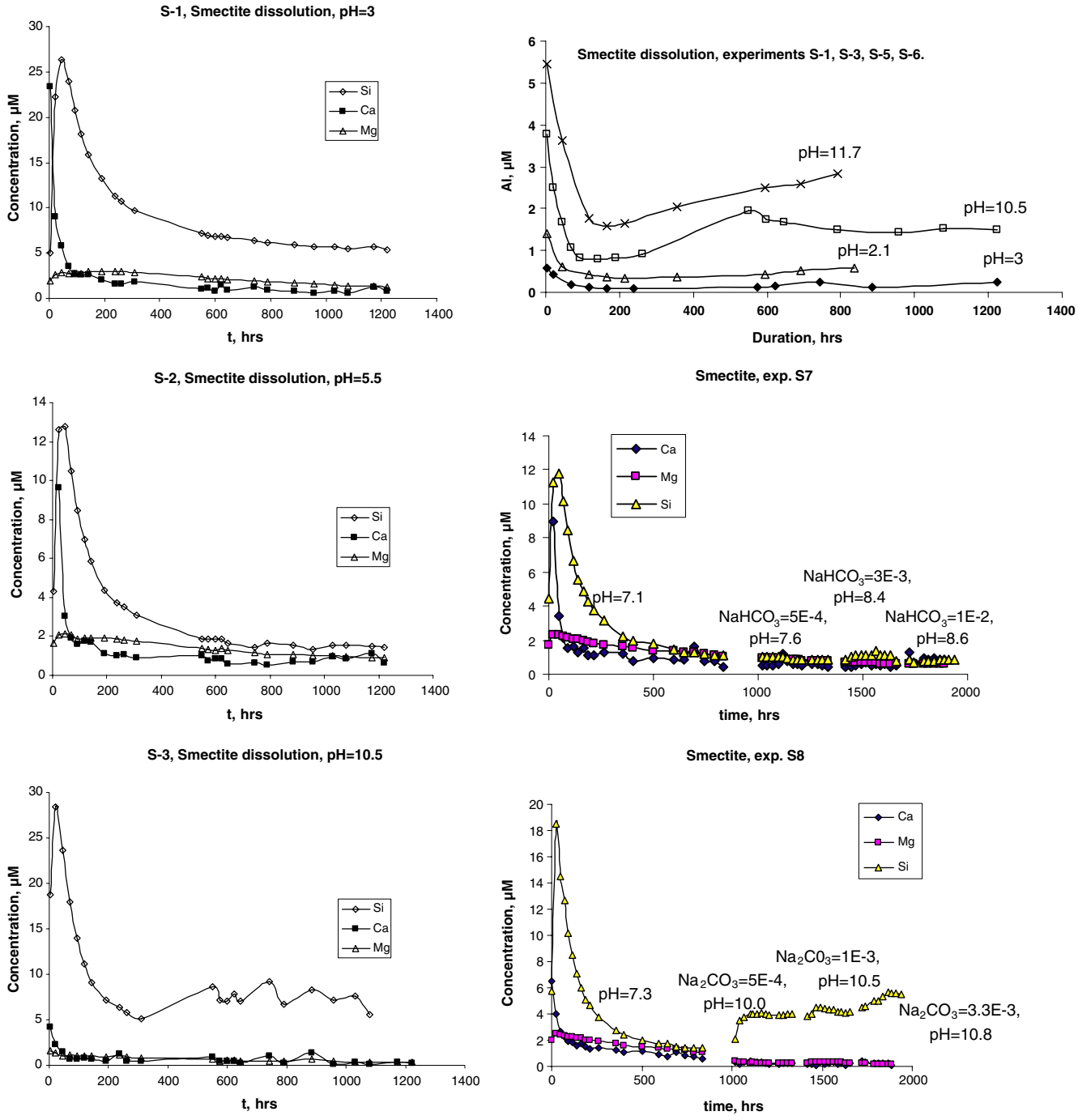

Fig. 8. Plots of concentrations in outlet solution as a function of elapsed time from the beginning of the reaction. Details of experiments are presented in Table 1.

At the same time, it is known that the residence time of water in soils varies between several hours to several days. Thus, the quantitative features of smectite dissolution revealed in the present study should be applicable to most natural environments of clay weathering.

The concentration range of various carboxylic ligands (acetic, oxalic, and citric) detected in soil solutions spans from 10^{-6} to 10^{-4} M (Hue et al., 1986; Hongve et al., 2000). Based on results of the present study, one can calculate the concentrations of ligands necessary to triple the rates of smectite at pH around 7. For most ligands, very high concentrations (0.1–0.01 M), are necessary to appreciably affect the rates. Although the threshold of rate-affecting concentrations for strong complexants such as aromatic compounds and chelates are lower ($n \cdot 10^{-3}$ M, Fig. 6 and 7), this is still three orders of magnitude higher than those ever detected in soil solutions or groundwaters. Thus, the effect of individual organic ligands on smectite mineral dissolution rates should be negligible under conditions of natural settings. The effect of bacterial metabolites

and components of cell envelopes even at their concentrations as high as 1–10 g/L is expected to be quite weak as glucuronic residues, glucosamine, and alginate either inhibit or do not affect the rates of both Si and Mg release from SWy-2 montmorillonite. This implies extremely low impact of soil biological activity and dissolved organic matter on the chemical weathering of basic rocks and their alteration products in natural settings. Such a hypothesis contradicts the well-established concept of rock weathering fluxes increase in the presence of vegetation and plants (Moulton and Berner, 1998; Moulton et al., 2000). However, it is important to note that, besides atmospheric precipitates, bedrocks and soil minerals, an important source of dissolved elements in rivers can be degrading plant litter (Polynov, 1944; Glazovskaya, 1956; Kovda, 1956). Although the contribution of the latter to the annual net loss of elements from ecosystems to surficial flow is still poorly quantified, recent estimations demonstrate that up to 60–80% of silica and cations annual fluxes in rivers draining basaltic rocks and their erosion products (smectite-rich soils) may originate from the degradation of plant litter (Derry et al., 2005; Pokrovsky et al., 2005b, respectively).

4. Concluding remarks

Knowledge of smectite reactivity assessed by various macroscopic and spectroscopic techniques allowed quantification of smectite dissolution over a wide range of pH at 25 °C in the presence of different ligands. Similar to other sheet silicates, in acidic to neutral solutions, Si-release rate increases with decrease of pH. At pH > 8.5, hydroxyl ions facilitate the release of Si. In contrast, non-steady-state release of Mg decreases linearly with pH with a slope of 0.09 non-stoichiometrically with respect to silica suggesting the important role of exchange reactions between structural Mg and protons.

It follows from the results of this study that the effect of nine naturally important organic ligands on smectite and, possibly, other Mg-bearing sheet silicate dissolution at concentrations relevant to those found in natural soil environments should be quite weak. In order to increase smectite dissolution rate by a factor of ~3, very high concentrations of most organic ligands (0.01–0.1 M) are required. This is in contrast to framework aluminosilicates whose dissolution is greatly enhanced in the presence of minor amount of organic acids forming strong surface and aqueous complexes with aluminium (Amhrein and Suarez, 1988; Lundström and Ohman, 1990; Fein et al., 1995; Oelkers and Schott, 1998; Oelkers and Gislason, 2001).

An important consequence of the relatively weak effect of bacterial cell components and microbial exometabolites on smectite (and, possibly, other Ca- and Mg-bearing clays) reactivity in aqueous solutions is that the impact of plants and biota on mineral chemical weathering in soils may be weaker than generally argued for (alumino)silicates. As a result, atmospheric CO_2 consumption on the land due to direct dissolution of soil clay minerals and Ca, Mg-associated transport of HCO_3^- is unlikely to be strongly influenced by organic ligands present in soil solutions.

Acknowledgments

The authors are grateful to Jordi Cama and Roy Wogelius for very thorough and constructive reviews of the manuscript. This work was supported by Young Researchers grant of CNRS-INSU "ATIP sur Programmes" allocated to O.P. and by the French National Program for Basic Research (ANR "ECCO" project ECOSPHERE CONTINENTALE: Processus et Modélisation). The authors thank D. Schild, P. Weidler and F. Friedrich for careful technical assistance with XRD, BET, and IR analyses, respectively. We are also grateful to A. Castillo and C. Causseraund for their continuous help with experimental and analytical parts of this study, respectively.

Associate Editor: Roy A. Wogelius

Appendix A

See Fig. 8.

References

Allison, J.D., Brown, D.S., Novo-Gradac, K.J. (1991) MINTEQA2/PRODEFA2, A geochemical assessment model for environmental systems: version 3.0 user's manual. U.S. EPA, Athens, GA, 106 p.

Amhrein, C., Suarez, D.L., 1988. The use of a surface complexation model to describe the kinetics of ligand-promoted dissolution of anorthite. *Geochim. Cosmochim. Acta* **52**, 2785–2793.

Amram, K., Ganor, J., 2005. The combined effect of pH and temperature on smectite dissolution rate under acidic conditions. *Geochim. Cosmochim. Acta* **69**, 2535–2546.

Bauer, A., Berger, G., 1998. Kaolinite and smectite dissolution rate in high molar KOH solutions at 35° and 80 °C. *Appl. Geochem.* **13**, 905–916.

Bauer, A., Velde, B., 1999. Smectite transformation in high molar KOH solutions. *Clay Miner.* **34**, 259–273.

Becker, U., Biswas, S., Kendall, T., Risthaus, P., Putnis, C.V., Pina, C.M., 2005. Interactions between mineral surfaces and dissolved species: from monovalent ions to complex organic molecules. *Am. J. Sci.* **305**, 791–825.

Berg, A., Banwart, S.A., 2000. Carbon dioxide mediated dissolution of Ca–feldspar: implications for silicate weathering. *Chem. Geol.* **163**, 25–42.

Berner, R.A., 1992. Weathering, plants and the long-term carbon cycle. *Geochim. Cosmochim. Acta* **56**, 3225–3231.

Bickmore, B., Bosbach, D., Hochella, M.F., Charlet, L., Rufe, E., 2001. In situ atomic force microscopy study of hectorite and nontronite dissolution: implications for phyllosilicate edge surface structures and dissolution mechanisms. *Am. Mineral.* **86**, 411–423.

Blum, A., Lasaga, A., 1988. Role of surface speciation in the low-temperature dissolution of minerals. *Nature* **331**, 431–433.

Blum, A.E., Stillings, L.L., 1995. Feldspar dissolution kinetics. In: White, A.F., Brantley, S.L. (Eds.), *Chemical Weathering Rates of Silicate Minerals*, vol. 31. Mineral. Soc. Am., pp. 291–351.

Bosbach, D., Charlet, L., Bickmore, B., Hochella, M.F., 2000. The dissolution of hectorite: in-situ, real-time observations using atomic force microscopy. *Am. Mineral.* **85**, 1209–1216.

Brady, P.V., Carroll, S.A., 1994. Direct effects of CO_2 and temperature on silicate weathering: possible implications for climate control. *Geochim. Cosmochim. Acta* **58**, 1853–1856.

Brady, P.V., Gíslason, S.R., 1997. Seafloor weathering controls on atmospheric CO_2 and global climate. *Geochim. Cosmochim. Acta* **61**, 965–973.

Brunauer, S., Emmett, P.H., Teller, E., 1932. Adsorption of gases in multimolecular layers. *J. Am. Chem. Soc.* **60**, 309–319.

Cama, J., Ayora, Ch., Lasaga, A.C., 1999. The deviation-from-equilibrium effect on dissolution rate and on apparent variations in activation energy. *Geochim. Cosmochim. Acta* **63**, 2481–2486.

Cama, J., Ganor, J., Ayora, C., Lasaga, A.C., 2000. Smectite dissolution kinetics at 80 °C and pH 8.8. *Geochim. Cosmochim. Acta* **64**, 2701–2717.

Cama, J., Metz, V., Ganor, J., 2002. The effect of pH and temperature on kaolinite dissolution rate under acidic conditions. *Geochim. Cosmochim. Acta* **66**, 3913–3926.

Cama, J., Ganor, J., 2006. The effects of organic acids on the dissolution of silicate minerals: a case study of oxalate catalysis of kaolinite dissolution. *Geochim. Cosmochim. Acta* **70**, 2191–2209.

Carroll, S.A., Walther, J.V., 1990. Kaolinite dissolution at 25 °C, 60 °C, and 80 °C. *Am. J. Sci.* **290**, 797–810.

Carroll-Webb, S.A., Walther, J.V., 1988. A surface complex reaction model for the pH-dependence of corundum and kaolinite dissolution rates. *Geochim. Cosmochim. Acta* **52**, 2609–2623.

Casey, W.H., Westrich, H.R., Arnold, G.W., 1988. Surface chemistry of labradorite feldspar reacted with aqueous solutions at pH = 2, 3 and 12. *Geochim. Cosmochim. Acta* **52**, 2795–2807.

Casey, W.H., Westrich, H.R., Banfield, J.F., Ferruzi, G., Arnold, G.W., 1993b. Leaching and reconstruction at the surfaces of dissolving chain-silicate minerals. *Nature* **366**, 253–256.

Charlet, L., Schindler, P.W., Spadini, L., Furrer, G., Zysset, M., 1993. Cation adsorption on oxides and clays: the aluminum case. *Aquatic Sci.* **55**, 291–303.

Devidal, J.-L., Schott, J., Dandurand, J.-L., 1997. An experimental study of kaolinite dissolution and precipitation kinetics as a function of chemical affinity and solution composition at 150 °C, 40 bars, and pH 2, 6.8, and 7.8. *Geochim. Cosmochim. Acta* **61**, 5165–5186.

Derry, L.A., Kurtz, A.C., Ziegler, K., Chadwick, O.A., 2005. Biological control of terrestrial silica cycling and export fluxes to watersheds. *Nature* **433**, 728–731.

Dupré, B., Dessert, C., Oliva, P., Goddéris, Y., Viers, J., Francois, L., Millot, R., Gaillardet, J., 2003. Rivers, chemical weathering and Earth's climate. *C.R. Geoscience* **335**, 1141–1160.

Fein, J.B., Gore, N., Marshall, D., Yassa, L., Loch, A., Brantley, S.L., 1995. The effect of aqueous complexation and gibbsite surface sites on the decarboxylation rate of malonate. *Geochim. Cosmochim. Acta* **59**, 5071–5080.

Ferrage, E., Tournassat, Ch., Rinnert, E., Lanson, B., 2005. Influence of pH on the interlayer cationic composition and hydration state of Ca–montmorillonite: Analytical chemistry, chemical modelling and XRD profile modelling study. *Geochim. Cosmochim. Acta* **69**, 2797–2812.

Furrer, G., Zysset, M., Schindler, P.W., 1993. Weathering kinetics of montmorillonite: Investigations in batch and mixed-flow reactors. In: Manning, D.A.C., Hall, P.L., Hughes, C.R. (Eds.), *Geochemistry of Clay-Pore Fluid Interactions*, vol. 13. Chapman & Hall, pp. 243–262.

Ganor, J., Mogollon, J.L., Lasaga, A.C., 1995. The effect of pH on kaolinite dissolution rates and on activation energy. *Geochim. Cosmochim. Acta* **59**, 1037–1052.

Ganor, J., Cama, J., Metz, V., 2003. Surface protonation data of kaolinite—reevaluation based on dissolution experiments. *J. Colloid Interface Sci.* **264**, 67–75.

Glazovskaya, M.A., 1956. Participation of plant ash in formation of small grains of erosion products and soils. In: Betechtin (Ed.), *Weathering Crust*. Issue 2 pp. 61–76.

Golubev, S.V., Pokrovsky, O.S., Schott, J., 2004. Laboratory weathering of Ca- and Mg-bearing silicates: Weak effect of CO_2 and organic ligands. Abstracts of the 13th annual V.M. Goldschmidt Conference. Suppl. *Geochim. Cosmochim. Acta*, 68/11S, p. A418.

Golubev, S.V., Pokrovsky, O.S., Schott, J., 2005. Effect of dissolved CO_2 on the dissolution kinetics of basic silicates at 25 °C. *Chem. Geol.* **217**, 227–238.

Högbom, A.G., 1894. On the probability of secular variations of atmospheric carbon dioxide (in Swedish). *Sven. Chem. Tidsskr.* **6**, 169–176.

Hongve, D., Van Hees, P.A.W., Lundstrom, U.S., 2000. Dissolved components in precipitation water percolated through forest litter. *Eur. J. Soil Sci.* **51**, 667–677.

Huang, W.H., Keller, W.D., 1971. Dissolution of clay minerals in dilute organic acids at room temperature. *Am. Mineral.* **56**, 1082–1095.

Hue, N.V., Craddock, G.R., Adams, F., 1986. Effect of organic acids on aluminum toxicity in subsoils. *Soil Sci. Soc. Am. J.* **50**, 28–34.

Huertas, F.J., Caballero, E., Jimenez de Cisneros, C., Linares, J., 2001. Kinetics of montmorillonite dissolution in granitic solutions. *Appl. Geochem.* **16**, 397–407.

Huertas, J.F., Chou, L., Wollast, R., 1998. Mechanism of kaolinite dissolution at room temperature and pressure: Part 1. Surface speciation. *Geochim. Cosmochim. Acta* **62**, 417–431.

Huertas, J.F., Chou, L., Wollast, R., 1999. Mechanism of kaolinite dissolution at room temperature and pressure: Part II: Kinetic study. *Geochim. Cosmochim. Acta* **63**, 3261–3275.

Kohler, S., Dufaud, F., Oelkers, E.H., 2003. An experimental study of illite dissolution kinetics as a function of pH from 1.4 to 12.4 and temperature from 5 to 50 °C. *Geochim. Cosmochim. Acta* **67**, 3583–3594.

Kohler, S.J., Bosbach, D., Oelkers, E.H., 2005. Do clay mineral dissolution rates reach steady state? *Geochim. Cosmochim. Acta* **69**, 1997–2006.

Koroleff, F., 1976. Determination of silicon. In: Grasshoff, K. (Ed.), *Methods of Seawater Analysis*. Verlag Chemie, pp. 149–158.

Kovda, V.A., 1956. Mineral composition of plants and soil formation. *Soviet Soil Sci. (Pochvovedenie) No* **1**, 6–38.

Lasaga, A.C., 1995. Fundamental approaches in describing mineral dissolution and precipitation rates. In: White, A.F., Brantley, S.L. (Eds.), Chemical Weathering Rates of Silicate Minerals. Rev. Mineral. 31, 23–86.

Lundström, U., Ohman, L.-O., 1990. Dissolution of feldspars in the presence of natural, organic solutes. *J. Soil Sci.* **41**, 359–369.

Martell, A.E., Smith, R.M., Motekaitis, R.J., 1997. Critically selected stability constants of metal complexes database. Version 3.0. Texas A & M University, College Station, TX.

Mermut, A.R., Cano, A.F., 2001. Baseline studies of the clay minerals society sourcece clays: chemical analyses of major elements. *Clay. Clay Miner.* **49**, 381–386.

Metz, V., Ganor, J., 2001. Stirring effect on kaolinite dissolution rate. *Geochim. Cosmochim. Acta* **65**, 3475–3490.

Metz, V., Amram, K., Ganor, J., 2005a. Stoichiometry of smectite dissolution reaction. *Geochim. Cosmochim. Acta* **69**, 1755–1772.

Metz, V., Raanan, H., Pieper, H., Bosbach, D., Ganor, J., 2005b. Towards the establishment of a reliable proxy fort he reactive surface area of smectite. *Geochim. Cosmochim. Acta* **69**, 2581–2591.

Moore, D.M., Reynolds Jr., R.C., 1997. *X-ray Diffraction and the Identification and Analysis of Clay Minerals*. Oxford University Press, p. 378.

Moulton, K.L., Berner, R.A., 1998. Quantification of the effect of plants on weathering: studies in Iceland. *Geology* **26**, 895–898.

Moulton, K.L., West, J., Berner, R.A., 2000. Solute flux and mineral mass balance approaches to the quantification of plant effects on silicate weathering. *Am. J. Sci.* **300**, 539–570.

Murphy, W.M., Helgeson, H.C., 1987. Thermodynamic and kinetic constraints on reaction rates among minerals and aqueous solutions: III. Activated complex and the pH-dependence of the rates of feldspar, pyroxene, wollastonite, and forsterite hydrolysis. *Geochim. Cosmochim. Acta* **51**, 3137–3153.

Nagy, K.L., Blum, A.E., Lasaga, A.C., 1991. Dissolution and precipitation kinetics of kaolinite at 80 °C and pH 3: The dependence on solution saturation state. *Am. J. Sci.* **291**, 649–686.

Nagy, K.L., 1995. Dissolution and precipitation kinetics of sheet silicates. In: White, A.F., Brantley, S.L. (Eds.), *Chemical Weathering Rates of Silicate Minerals*, vol. 31. Mineral. Soc. Am., pp. 173–233.

Oelkers, E.H., Schott, J., 1998. Does organic acid adsorption affect alkali–feldspar dissolution rates? *Chem. Geol.* **151**, 235–245.

Oelkers, E.H., Schott, J., 2001. An experimental study of enstatite dissolution rates as a function of pH, temperature, and aqueous Mg and Si concentration, and the mechanism of pyroxene/pyroxenoid dissolution. *Geochim. Cosmochim. Acta* **65**, 1219–1231.

Oelkers, E.H., Gislason, S.R., 2001. The mechanism, rates and consequences of basaltic glass dissolution: I. An experimental study of the dissolution rates of basaltic glass as a function of aqueous Al, Si and oxalic acid concentration at 25 °C and pH = 3 and 11. *Geochim. Cosmochim. Acta* **65**, 3671–3681.

Pokrovski, G.S., Schott, J., 1998. Experimental study of the complexation of silicon and germanium with aqueous organic species: Implications for germanium and silicon transport and Ge/Si ratio in natural waters. *Geochim. Cosmochim. Acta* **62**, 3413–3428.

Pokrovsky, O.S., Schott, J., 2000a. Forsterite surface composition in aqueous solutions: a combined potentiometric, electrokinetic, and spectroscopic approach. *Geochim. Cosmochim. Acta* **64**, 3299–3312.

Pokrovsky, O.S., Schott, J., 2000b. Kinetics and mechanism of forsterite dissolution at 25 °C and pH from 1 to 12. *Geochim.Cosmochim. Acta* **64**, 3313–3325.

Pokrovsky, O.S., Schott, J., 2001. Kinetics and mechanism of dolomite dissolution in neutral to alkaline solutions revisited. *Am. J. Sci.* **301**, 597–626.

Pokrovsky, O.S., Schott, J., 2004. Experimental study of brucite dissolution and precipitation in aqueous solutions. Surface speciation and chemical affinity control. *Geochim. Cosmochim. Acta* **68**, 31–45.

Pokrovsky, O.S., Golubev, S.V., Schott, J., 2004. Impact of dissolved organics on mineral dissolution kinetics: Towards a predictive model for Ca- and Mg-bearing oxides, carbonates and silicates. Abstracts of the 13th annual V.M. Goldschmidt Conference. Suppl. Geochim. Cosmochim. Acta 68/11S, p. A141.

Pokrovsky, O.S., Schott, J., Castillo, A., 2005a. Kinetics of brucite dissolution at 25 °C in the presence of organic and inorganic ligands and divalent metals. *Geochim. Cosmochim. Acta* **69**, 905–918.

Pokrovsky, O.S., Schott, J., Kudryavtzev, D.I., Dupré, B., 2005b. Basalts weathering in Central Siberia under permafrost conditions. *Geochim. Cosmochim. Acta* **69**, 5659–5680.

Polynov, B.B., 1944. Modern objects of weathering study (Sovremennye zadachi ucheniya o vyvetrivanii), Izv. *Acad. Nauk SSSR, Ser. Geol.* **2**, 3–14.

Rogers, J.R., Bennett, Ph.C., 2004. Mineral stimulation of subsurface microorganisms: release of limiting nutrients from silicates. *Chem. Geol.* **203**, 91–108.

Sawhney, B.L., Stilwell, D.E., 1994. Dissolution and elemental analyses of mineral water-interactions. In: Amonette, J.E., Zelazny, L.W. (Eds.), *Quantitative Methods in Soil Mineralogy*. Soil Science Society of America, pp. 49–82.

Schindler, P.W., Stumm, W., 1987. The surface chemistry of oxides, hydroxides, and oxide minerals. In: Stumm, W. (Ed.), *Aquatic Surface Chemistry*. Wiley, pp. 337–365.

Schnitzer, M., Kodama, H., 1976. The dissolution of mica by fulvic acid. *Geoderma* **15**, 381–391.

Stadler, M., Schindler, P.W., 1993. Modeling of H^+ and Cu^{2+} adsorption on calcium–montmorillonite. *Clay. Clay Miner.* **41**, 288–296.

Stucki, J.W., Golden, D.C., Roth, C.B., 1984. Effects of reduction and reoxidation of structural iron on the surface charge dissolution of dioctahedral smectites. *Clay. Clay Miner.* **32**, 350–356.

Stumm, W., 1992. *Chemistry of the Solid–Water Interface*. Wiley.

Stumm, W., 1997. Reactivity at the mineral–water interface: dissolution and inhibition. *Colloids Surf. A* **120**, 143–166.

Sverdrup, H., 1990. *The Kinetics of Base Cation Release due to Chemical Weathering*. Lund University Press.

Welch, S.A., Vandevivere, P., 1994. Effect of microbial and other naturally occurring polymers on mineral dissolution. *Geomicrobiol. J.* **12**, 227–238.

Welch, S.A., Barker, W.W., Banfield, J.F., 1999. Microbial extracellular polysaccharides and plagioclase dissolution. *Geochim. Cosmochim. Acta* **63**, 1405–1419.

Wieland, E., Stumm, W., 1992. Dissolution kinetics of kaolinite in acidic aqueous solutions at 25 °C. *Geochim. Cosmochim. Acta* **56**, 3339–3355.

Wilson, J., Savage, D., Cuadros, J., Shibata, M., Ragnarsdottir, K.V., 2006. The effect of iron on montmorillonite stability. (I) Background and thermodynamic considerations. *Geochim. Cosmochim. Acta* **70**, 306–322.

Wogelius, R.A., Walther, J.V., 1991. Forsterite dissolution at 25 °C: Effects of pH, CO_2, and organic acids. *Geochim. Cosmochim. Acta* **55**, 943–954.

Wolery, T.J., 1983. EQ3NR, a computer program for geochemical aqueous speciation—solubility calculations: users guide and documentation, UCRL-53414. Lawrence Livermore National Laboratory.

Zysset, M., Schindler, P.W., 1996. The proton-promoted dissolution kinetics of K–montmorillonite. *Geochim. Cosmochim. Acta* **60**, 921–931.